Research Square

Preprints are preliminary reports that have not undergone peer review.
They should not be considered conclusive, used to inform clinical practice,
or referenced by the media as validated information.

High-Entropy Spinel Oxide Catalyst for Selective CO_2 hydrogenation to Methanol

Mingyue Ding

dingmy@whu.edu.cn

Wuhan University https://orcid.org/0000-0001-8769-4153

Siyi Huang

Wuhan University

Ting Zeng

School of Power and Mechanical Engineering, Wuhan University, Wuhan, 430072, China

Di Xu

Wuhan University

Guoqiang Hou

Wuhan University

Yangyang Li

School of Power and Mechanical Engineering, Wuhan University, Wuhan, 430072, China

Ruosong He

China University of Petroleum (East China)

Hanzhu Zhang

Wuhan Universi

Jiajun Peng

School of Power and Mechanical Engineering, Wuhan University, Wuhan, 430072, China

Hongmei Yang

Shanxi Key Laboratory of Coal-based Synthetic Oil Product Testing, Changzhi, 046000, China

Yao Wang

School of Power and Mechanical Engineering, Wuhan University, Wuhan, 430072, China

Chun-Ran Chang

Xi'an Jiaotong University

Xiang-Kui Gu

Wuhan University https://orcid.org/0000-0001-6537-7026

Article

Keywords: CO2 hydrogenation, methanol synthesis, high-entropy, spinel oxide, phase transformation

Posted Date: June 1st, 2026

DOI: https://doi.org/10.21203/rs.3.rs-9578588/v1

License: This work is licensed under a Creative Commons Attribution 4.0 International License.
Read Full License

Additional Declarations: There is **NO** Competing Interest.

Abstract

Methanol synthesis via CO_2 hydrogenation stands as a cornerstone technology for large-scale CO_2 valorization and green H_2 storage, yet hindered by the lack of innovative catalyst systems, facing the challenge of activity-stability trade-off. Herein, we represent the first report on a new $ZnCoAlFeGaO_x$ high-entropy oxide (HEO) catalyst for CO_2 hydrogenation to methanol production. The successful construction of HEO, featuring the incorporation of multiple oxyphilic metal elements, induces substantial charge redistribution, which reinforces metal-oxygen bonding and confers exceptional structural stability under reaction conditions. Concurrently, the high-entropy spinel triggers pronounced lattice distortion and nanoscale grain refinement, significantly increasing the density of active sites and enhancing the intrinsic catalytic activity. Benefiting from these synergistic effects, HEO catalyst achieves an unprecedented methanol space time yield (STY) of 498 $g_{MeOH}{\cdot}kg_{cat}^{-1}{\cdot}h^{-1}$ at 73.3% selectivity, together with excellent long-term stability for 120 h, far outperforming its low-entropy and medium-entropy counterparts, as well as most reported oxide-based catalysts. This work establishes a feasible and robust strategy for the development of high-performance and durable CO_2 hydrogenation catalytic systems, and deeply clarifies the origin of the high-entropy effect in governing catalytic activity and stability.

Introduction

The escalating climate crisis and imperative to decarbonize industrial systems have elevated CO_2 catalytic conversion into a cornerstone of sustainable chemistry[1,2]. Methanol, a versatile platform chemical, serves not only a clean fuel but also as a fundamental feedstock for the production of numerous high-value chemicals[3,4]. Moreover, it acts as an excellent medium for hydrogen storage and transportation, enabling the large-scale utilization of intermittent renewable H_2[5]. In this context, methanol production via CO_2 catalytic hydrogenation directly bridges the development of the green H_2 industry and the implementation of carbon neutrality goals. Cu-based catalysts have long been dominant in this field owing to their decent activity and cost effectiveness, yet severe deactivation arising from Cu sintering under harsh high-temperature, H_2-rich and humid conditions, remains a fundamental bottleneck[6]. To date, no effective solution has been established to overcome this limitation. Therefore, novel catalyst systems are urgently needed to address the bottleneck of simultaneously balancing CO_2 conversion, methanol selectivity, and long-term stability.

Composite oxide catalysts, including fluorite-type ($InZrO_x$, $ZnZrO_x$, $GaZrO_x$)[7,8] and spinel-type ($ZnFe_2O_4$, $ZnAl_2O_4$, $ZnCr_2O_4$)[9–12] oxides, have garnered extensive attention due to their high methanol selectivity and structural stability. However, such catalysts generally suffer from mismatched activation capabilities toward CO_2 and H_2, resulting in intrinsically limited catalytic activity[13–15]. While compositional modulation and synthetic optimization can partially improve the synergy between CO_2 and H_2 activation, the inherent lattice mismatch between binary metal oxides renders them highly susceptible to

irreversible phase transformation under reaction conditions, leading to rapid decline of methanol productivity[16–18]. For instance, in $GaZrO_x$ catalysts, excessive Ga doping (> 20%) triggers a phase transition from a single-phase solid solution to mixed phases of ZrO_2 and Ga_2O_3, drastically reducing methanol yield by more than 50%[16]. Moreover, low-valence surface metals such as Zn, Ga, and In tend to migrate, agglomerate or even be over-reduced under reaction conditions, promoting the formation of numerous by-products including CO and CH_4[19–21]. Notably, recent studies have revealed that phase transformation of the spinel lattice can induce an abrupt collapse of methanol selectivity from 96.1% to a mere 1.2%[10]. Consequently, overcoming the irreversible phase transformation of composite oxide catalysts under reaction conditions becomes the key point for resolving the activity-stability trade-off.

High-entropy oxides (HEO) are defined as single-phase solid solutions containing five or more metal cations in an approximately equimolar ratio[22–25]. Benefiting from their unique characteristics including the high-entropy effect, lattice distortion effect, sluggish diffusion effect, and cocktail effect, high-entropy materials exhibit unprecedented physicochemical properties, thus gaining increasing attention in heterogeneous catalysis[26–28]. For instance, Li[29] et al. developed a fluorite-type high-entropy catalyst $Cu_2Zn_1Al_{0.5}Ce_5Zr_{0.5}O_x$ for the reverse water-gas shift (RWGS) reaction, in which the high-entropy lattice effectively suppressed Cu sintering and enabled a high CO production rate of 417.2 $mmol \cdot g^{-1} \cdot h^{-1}$ with good stability over 72 h of continuous testing. This distinctive structure provides a versatile platform to break the inherent activity-stability trade-off in conventional catalysts. Nevertheless, the application of HEO in selective CO_2 hydrogenation to methanol remains largely unexplored. More importantly, the intrinsic catalytic mechanism of the high-entropy effect remains poorly understood, hindering the rational design of advanced HEO catalysts.

In this work, we represent the first report on a high-entropy spinel catalyst that successfully breaks the inherent activity-stability trade-off in CO_2 hydrogenation to methanol. The optimized $ZnCoAlFeGaO_x$ catalyst delivers an unprecedented methanol space time yield (STY) of 498 $g_{MeOH} \cdot kg_{cat}^{-1} \cdot h^{-1}$ at 73.3% selectivity, together with excellent stability for 120 h. This performance far surpasses that of its low-entropy and medium-entropy analogs, as well as most reported oxide-based catalysts. Experimental and theoretical studies reveal the intrinsic mechanism underlying the superior performance of the HEO catalyst. Specifically, the incorporation of oxyphilic elements induces significant charge redistribution, which reinforces metal-oxygen bonding and confers exceptional structural stability under reaction conditions. In addition, the high-entropy spinel lattice triggers lattice distortion and nanoscale grain refinement, which significantly increase the density of active sites and enhance the intrinsic catalytic activity. This study not only opens a reliable avenue toward high-performance and durable CO_2 hydrogenation catalytic systems, but also deeply clarifies the intrinsic catalytic mechanism of the high-entropy effect, providing valuable theoretical guidance for the rational design of advanced high-entropy oxide catalysts.

Results and discussion

3.1. Structural characterization of catalysts

A series of spinel-type catalysts ($ZnFeO_x$, $ZnFeGaO_x$, $ZnCoFeGaO_x$, and $ZnCoAlFeGaO_x$) were synthesized via a polyvinylpyrrolidone (PVP)-templated method[29] (Figure S1). According to the classification criteria of low-entropy oxide (LEO, < 1.0R), medium-entropy oxide (MEO, 1.0-1.5R), and high-entropy oxide (HEO, > 1.5R), these catalysts were denoted as ZF-LEO, ZFG-MEO, ZCFG-MEO, and ZCAFG-HEO, respectively (Fig. 1a). Powder X-ray diffraction (XRD) confirms that all catalysts exhibit a pure single-phase spinel structure without detectable impurity phases (Fig. 1b). As the metal constituent diversity increases from binary to quinary, the diffraction peaks systematically shift toward higher angles, providing direct evidence of lattice contraction, originated from mismatched ionic radii, charge states, and coordination preferences of the multiple cation species[30]. Meanwhile, the weakened and broadened diffraction peaks imply suppressed grain growth and reduced grain size with rising configurational entropy. XRD Rietveld refinement further verifies that all diffraction peaks are attributed to the Fd_3m space group, with refined lattice parameters decreasing from 8.447 Å for ZF-LEO to 8.212 Å for ZCAFG-HEO (Figs. 1c and S2, Table S1).

Scanning electron microscopy (SEM) images reveal that all samples consist of nanosheet assemblies formed by aggregated nanoparticles (Figure S3). Transmission electron microscopy (TEM) images show that ZF-LEO possesses a wide size distribution ranging from 10 to 100 nm, with an average diameter of approximately 48.5 nm (Figure S4). In striking contrast, ZCAFG-HEO displays a more uniform and smaller particle size distribution with an average diameter of only 10.4 nm, reflecting the crystallite refinement induced by high-entropy effect as confirmed by XRD[30] (Fig. 1d). This nanoscale grain refinement endows ZCAFG-HEO with a higher specific surface area and CO_2 adsorption capacity relative to LEO and MEO catalysts (Figures S5 and S6, Table S2). High-resolution TEM (HRTEM) of ZCAFG-HEO reveals lattice spacings of 0.250, 0.292, and 0.480 nm (Fig. 1e), corresponding to the (311), (200), and (111) planes of the spinel structure[31]. These interplanar distances are slightly contracted relative to those in ZF-LEO (Figure S7), consistent with the lattice contraction indicated by XRD. Furthermore, energy dispersive X-ray spectroscopy (EDS) elemental mapping validates the uniform distribution of all elements at the nanoscale (Fig. 1d and Figure S8). Collectively, these characterizations confirm the successful fabrication of a phase-pure, compositionally uniform high-entropy spinel catalyst.

X-ray absorption spectroscopy (XAS) was employed to probe the electronic structure and local coordination environment of ZF-LEO and ZCAFG-HEO. Fe K-edge XANES spectra show that the absorption edges of both catalysts lie between those of Fe foil and Fe_2O_3, with spectral features similar to Fe_2O_3 (Fig. 1f). Notably, the absorption edge of ZCAFG-HEO shifts toward lower energy relative to ZF-LEO, indicating increased electron density at Fe centers. A similar trend is observed for the Zn K-edge XANES spectra (Figure S9), corroborating pronounced charge redistribution within the high-entropy system. Quantitative EXAFS fitting in R-space reveals a clear shortening of the Fe-O bond length in ZCAFG-HEO (Fig. 1g and Table S3). Moreover, ZCAFG-HEO exhibits unique Fe-(O)-M scattering contributions characteristic of the multi-elemental spinel lattice, distinct from the Fe-(O)-Fe and Fe-(O)-

Zn coordination environments in ZF-LEO. Similar structural variations are also identified in Zn-O and other coordination shells (Figure S10 and Table S4). Wavelet transform EXAFS (WT-EXAFS) further resolves subtle differences in the local coordination environment (Figs. 1h and S11). X-ray photoelectron spectroscopy (XPS) provides additional evidence for charge redistribution. ZCAFG-HEO shows a higher Fe^{2+} fraction (57.1%) compared to ZF-LEO (35.7%), indicating an electron-enrich nature of Fe sites (Figure S12). Meanwhile, the O 1s binding energy in ZCAFG-HEO shifts markedly toward higher values compared to ZF-LEO (Figure S13). These observations collectively demonstrate that the diverse atomic sizes and modulated M-O bonding environments in HEO induce substantial internal charge redistribution, characterized by electron transfer from oxygen to Fe centers[32,33].

To elucidate the microscopic mechanism of charge redistribution, theoretical calculations were performed on two constructed $ZnFe_2O_4$ (ZF-LEO) and $ZnCoAlFeGaO_4$ (ZCAFG-HEO) models (Supporting Methods). Crystal Orbital Hamiltonian Populations (COHP) analysis reveals that the oxyphilic dopants Ga and Al in ZCAFG-HEO exhibit higher bonding affinity with oxygen, as reflected by the negatively integrated COHP (-ICOHP) values of approximately 2.60 eV (Fig. 1i), substantially exceeding the strengths of intrinsic Zn-O and Fe-O bonds in ZF-LEO (< 1.70 eV). For Fe-O interaction, charge density difference and electron localization function (ELF) analyses show that oxygen bonded to Fe on the ZCAFG-HEO surface gains only 1.04 |e|, indicating a reduced electron density on lattice oxygen compared to 1.10 |e| in ZF-LEO (Figure S14). Meanwhile, Fe atom loses fewer electrons (1.58 |e| for ZCAFG-HEO v.s. 1.60 |e| for ZF-LEO), resulting in electron accumulation around Fe center and effectively strengthening the Fe-O interaction. These results establish that the incorporation of strongly oxyphilic elements in ZCAFG-HEO reduces electron transfer between O and Fe, induces significant charge redistribution, and ultimately shortens Fe-O bond (Figure S15), consistent with experimental observations.

Raman spectroscopy was further utilized to probe Fe-O bonding variations (Figure S16). The characteristic peak corresponding to Fe-O bond[34] in ZF-LEO appears at 650 cm^{-1}. In contrast, this peak in ZCAFG-HEO exhibits a distinct blue shift to approximately 680 cm^{-1}, indicating an increased bond force constant and strengthened Fe-O bond[35]. As a result, the reduction temperature of ZCAFG-HEO increases by more than 40°C relative to LEO catalyst, accompanied by a lowered reduction extent (Figure S17). This ensures the structural integrity of spinel under reducing atmosphere. Notably, ZnFe-based spinel is highly prone to phase transformation under CO_2 hydrogenation conditions, resulting in product selectivity reversal[10]. In contrast, the electron redistribution driven by oxyphilic element introduction in HEO significantly reinforces Fe-O bonding and confers exceptional structural stability to the ZCAFG-HEO catalyst.

3.2. Catalytic performance of CO_2 hydrogenation to methanol

CO_2 hydrogenation performance was evaluated at 5 MPa, 24,000 $mL \cdot g^{-1} \cdot h^{-1}$ and 280–360°C. All spinel catalysts show increasing CO_2 conversion with rising temperature, yet exhibit drastically different product selectivity. For binary low-entropy ZF-LEO (Fig. 2a), CO_2 conversion increases from 0.2% to 8.1% with rising temperature, accompanied by a continuous drop in methanol selectivity from 99.3% to 11.1%, while CO selectivity surges to 68.6%. This indicates that the reverse water-gas shift (RWGS) reaction becomes dominant under high-temperatures. Notably, ZF-LEO generates substantial hydrocarbon byproducts (CH_4 and C_2^+ hydrocarbons), with combined selectivity exceeding 20% above 320°C, reflecting excessive hydrogenation and C-C coupling side reactions. Correspondingly, its maximum methanol space-time yield (STY) is only 74 $g_{MeOH} \cdot kg_{cat}^{-1} \cdot h^{-1}$. The medium-entropy ZFG-MEO and ZCFG-MEO catalysts display improved methanol selectivity at comparable CO_2 conversion (Figures S18 and S19), affording enhanced methanol STY of 270 and 219 $g_{MeOH} \cdot kg_{cat}^{-1} \cdot h^{-1}$, respectively, while suppressing hydrocarbon selectivity to below 4.8%.

For quinary high-entropy ZCAFG-HEO (Fig. 2b), CO_2 conversion is further enhanced at similar methanol selectivity relative to MEO catalysts, with hydrocarbon selectivity maintained below 1% even at 360°C, demonstrating nearly complete suppression of excessive hydrogenation and C-C coupling side reactions. A direct performance comparison at 320°C highlights that methanol selectivity dramatically increases from ~ 25% for LEO catalyst to ~ 70% for MEO and HEO catalysts (Fig. 2c and Table S5). Impressively, ZCAFG-HEO achieves the highest methanol STY of 381 $g_{MeOH} \cdot kg_{cat}^{-1} \cdot h^{-1}$, representing a 6.5-fold enhancement over ZF-LEO (59 $g_{MeOH} \cdot kg_{cat}^{-1} \cdot h^{-1}$) and a 2.2-fold enhancement over ZCFG-MEO (174 $g_{MeOH} \cdot kg_{cat}^{-1} \cdot h^{-1}$). After optimizing the reaction conditions, ZCAFG-HEO realizes a remarkable methanol STY of 498 $g_{MeOH} \cdot kg_{cat}^{-1} \cdot h^{-1}$ with 73.3% selectivity (Figure S20), far exceeding previously reported spinel catalysts, and on par with state-of-art oxide-based catalysts (Fig. 2d and Table S6). These results underscore the efficacy of the high-entropy strategy in constructing highly active spinel catalysts for CO_2 valorization.

Kinetic analysis based on the Arrhenius aquation for CO_2 hydrogenation to methanol was conducted to study the origins of enhanced catalytic activity (Figs. 2e-f and Table S7). The apparent activation energy (Ea) gradually increases with configurational entropy: 88.55 $kJ \cdot mol^{-1}$ for ZF-LEO, 92.35 $kJ \cdot mol^{-1}$ for ZFG-MEO, 98.91 $kJ \cdot mol^{-1}$ for ZCFG-MEO, and 114.66 $kJ \cdot mol^{-1}$ for ZCAFG-HEO (Fig. 2e and Table S8). Despite possessing the highest Ea, ZCAFG-HEO achieves an overall reaction rate 6.5-fold that of ZF-LEO, a trend unaccounted for by apparent activation energy alone. Correspondingly, the pre-exponential factor significantly increases from 4.11×10^6 for ZF-LEO to 2.21×10^7 for ZFG-MEO, 9.13×10^7 for ZCFG-MEO, and an exceptional 5.09×10^9 for ZCAFG-HEO, representing a 2–3 orders-of-magnitude enhancement relative to other counterparts (Fig. 2f and Table S8). The extraordinarily high pre-exponential factor overrides the energy barrier effect, accounting for the superior methanol synthesis activity[36–39]. This behavior correlates well with the typical structural merits of high-entropy materials: nanoscale grain refinement,

enlarged specific surface area, and increased active site density, which promote reactant adsorption, activation, and surface reaction kinetics.

Long-term stability tests were further conducted on ZF-LEO, ZCFG-MEO, and ZCAFG-HEO at 320°C, 5 MPa and 36,000 $mL \cdot g^{-1} \cdot h^{-1}$ (Fig. 3a). Within the first hour, the methanol selectivity of ZF-LEO abruptly drops from 47.1% to 13.9%, and further declines to 7.9% after 10 h, while its STY decreases from 103 to 57 $g_{MeOH} \cdot kg_{cat}^{-1} \cdot h^{-1}$. ZCFG-MEO exhibits slightly improved stability versus ZF-LEO, yet still suffers significant degradation in methanol selectivity and STY within 5 h, with STY falling from 236 to 157 $g_{MeOH} \cdot kg_{cat}^{-1} \cdot h^{-1}$ over 35 h. In stark contrast, ZCAFG-HEO maintains exceptional stability during a continuous 120 h test (Figs. 3a and S21), sustaining methanol selectivity at around 70% and methanol STY above 400 $g_{MeOH} \cdot kg_{cat}^{-1} \cdot h^{-1}$. These results fully demonstrate that the ZCAFG-HEO catalyst integrates superior methanol synthesis activity, high methanol selectivity, and outstanding long-term stability, far outperforming its LEO and MEO counterparts.

To elucidate the origins of catalytic performance discrepancies, a series of characterizations were performed on the spent catalysts to probe their structural evolution. XRD patterns indicate that spent ZCFG-MEO and ZCAFG-HEO maintain their pristine spinel structure (Fig. 3b). In comparison, spent ZF-LEO exhibits two new diffraction peaks at 31.7° and 36.2°, corresponding to the (100) and (101) planes of ZnO (JCPDS no. 36-1451), suggesting the irreversible phase separation of ZnO from the spinel bulk after CO_2 hydrogenation reaction. XPS analysis of the spent catalysts provides further insights (Fig. 3c). In addition to Fe^{2+}/Fe^{3+} signals, a distinct peak at 708.1 eV, assigned to FeC_x species, is observed on both ZF-LEO and ZCFG-MEO[10,40]. This indicates partial spinel decomposition into ZnO and FeC_x after catalytic reaction. Notably, the FeC_x signal intensity is weakened in ZCFG-MEO and completely absent in ZCAFG-HEO. Mössbauer spectroscopy (Fig. 3d) reveals that spent ZCAFG-HEO is dominated by Fe^{3+} (90.11%) with a minor Fe^{2+} component (9.89%), with no detectable Fe^0 or FeC_x phases[41,42]. These results confirm that the robust spinel structure of ZCAFG-HEO remains intact under reaction conditions, enabling sustained high methanol selectivity.

TEM characterization provides direct visualization of structural evolution. Spent ZCAFG-HEO possesses uniformly sized nanoparticles of approximately 12.0 nm (Figure S22), without obvious agglomeration relative to the fresh catalyst (10.4 nm). HRTEM reveals only spinel-specific (220) and (311) crystal planes, and EDS elemental mapping further shows uniform dispersion of Zn, Co, Al, Fe, Ga, and O elements without segregation (Figs. 3e and 3f). By contrast, spent ZF-LEO suffers severe particle sintering and agglomeration, with HRTEM identifying lattice spacings of ZnO, Fe_3O_4 and Fe_5C_2 phases (Figs. 3g and S23). Meanwhile, EDS mapping further reveals distinct demarcation between Zn and Fe elements (Figs. 3h and S24), confirming severe phase transformation of the $ZnFe_2O_4$ spinel into ZnO, Fe_3O_4 and Fe_5C_2 after CO_2 hydrogenation reaction.

These findings establish a direct structure-performance relationship that the irreversible phase transformation of ZF-LEO from spinel to ZnO, Fe_3O_4 and Fe_5C_2 drives selectivity reversal from methanol to CO and hydrocarbons. In ZCAFG-HEO, the oxyphilic element introduction induces extensive charge redistribution, strengthens Fe-O bonding, and stabilizes the spinel lattice, thus preserving high methanol selectivity. Furthermore, high-entropy-induced grain refinement and lattice distortion generate a high density of active sites. As a result, ZCAFG-HEO maintains ~ 70% methanol selectivity with STY consistently exceeding 400 $g_{MeOH}{\cdot}kg_{cat}^{-1}{\cdot}h^{-1}$ over 120 h, achieving superior catalytic activity and long-term stability.

3.3. Evolution of Catalyst Structure and Reaction Pathway

In-situ XRD and diffuse reflectance infrared Fourier transform spectroscopy (DRIFTS) were employed to establish the dynamic correlation between catalyst structural evolution and reaction pathway switching under CO_2 hydrogenation conditions for ZF-LEO and ZCAFG-HEO catalysts. *In-situ* CO_2 hydrogenation XRD patterns are shown in Figs. 4a-b. At 300–350°C, ZF-LEO maintains characteristic diffraction peaks of the $ZnFe_2O_4$ spinel phase. Upon heating to 400°C, new diffraction peaks corresponding to ZnO emerge, signaling the onset of spinel phase separation. With further temperature elevation, the peak intensity of ZnO strengthens, while spinel peaks weaken and shift toward higher angles (from 35.0° to 35.1°), suggesting partial reduction and transformation of $ZnFe_2O_4$ into Fe_3O_4. The Fe_3O_4 phase exhibits high intrinsic RWGS activity, explaining the elevated CO selectivity over ZF-LEO[10,43]. Substantial CO production simultaneously promotes the formation of FeC_x species, exacerbating methanol selectivity loss. In marked contrast, ZCAFG-HEO displays only minor shifts and intensity variations upon heating from 300°C to 500°C, with no phase separation detected (Figs. 4c-d). Even maintaining at 500°C for 20 h, the spinel structure remains fully preserved, confirming its exceptional intrinsic structural robustness.

In-situ CO_2 hydrogenation DRIFTS was then conducted to track reaction pathway changes alongside structural evolution. As shown in Figs. 4e-f and Figure S25, when the reactant gas is introduced into ZF-LEO catalyst, CO_2 and H_2 molecules are activated on the catalyst surface, forming CO_3*/HCO_3* species (1430/1268 cm^{-1})[12,44]. Meanwhile, characteristic peaks of HCOO* (1370, 1586, 2870, 2983 cm^{-1}) and CH_3O* (2953 cm^{-1}) intermediates appear, which are derived from CO_3*/HCO_3* hydrogenation, demonstrating evidencing methanol synthesis in the initial reaction stage[7,11,45]. As the reaction proceeds, HCOO* and CH_3O* are gradually consumed, accompanied by the formation and accumulation of gaseous CO (2101, 2172 cm^{-1}) and CH_4 (3018 cm^{-1}), confirming the dominance of RWGS and methanation side reactions[46,47]. Subsequent switching to H_2/N_2 accelerates spinel transformation into Fe_3O_4 or even Fe^0, resulting in complete depletion of HCOO* and CH_3O* intermediates within 10 min and a continuous enhancement of CH_4 signal. This reveals a clear reaction pathway shift from HCOO*-dominated selective methanol synthesis to RWGS and methanation side reactions as the spinel structure transition. For ZCAFG-HEO catalyst (Figs. 4g-h and S26), HCOO* species accumulate steadily with continuous growth of CH_3O* species. Upon switching to H_2/N_2, the conversion of HCOO* to CH_3O*

is obviously accelerated, and no CH_4 signal is detected throughout the reaction. These results confirm that methanol synthesis reaction via HCOO* intermediate dominates on ZCAFG-HEO.

Overall, these *in-situ* test results confirm that both catalysts initially drive CO_2 hydrogenation to methanol via the HCOO* pathway. However, ZF-LEO undergoes progressive pathway switching toward RWGS and methanation due to irreversible structural transformation from $ZnFe_2O_4$ spinel into Fe_3O_4, ZnO and Fe_5C_2. In contrast, the structurally stable ZCAFG-HEO preserves the selective methanol synthesis pathway throughout the reaction, enabling consistent high performance.

3.4. Stability Mechanism from theoretical perspective

To gain atomic-level insights into the exceptional stability of the quinary high-entropy spinel surface, we constructed binary $ZnFe_2O_4$(111) surface, named as ZF-LEO, and quinary $ZnCoAlFeGaO_4$(111) surface (named as ZCAFG-HEO) through bulk doping (Figure S27) corresponding to the experimental compositions. Given the well-established role of Fe coordination and stability in governing CO_2 hydrogenation selectivity, we focused on the dynamic behavior of Fe segregation and migration on both surfaces. On the ZF-LEO surface, an Fe atom initially coordinates with three surface O atoms, passing through a transition state coordinated with two surface O atoms, eventually migrating to form a metastable Fe adatom on the surface (Figure S28). This process requires overcoming an energy barrier of only 0.83 eV with a reaction energy of 0.26 eV (Fig. 5a), which is considered facile under typical reaction temperatures around 300°C. In contrast, Fe migration and segregation are kinetically hindered on the ZCAFG-HEO surface, where the energy barrier increases by 0.31 eV over an Al lattice (Al_L) site and even reaches 2.59 eV over a Ga lattice (Ga_L) site (Fig. 5a and Figure S29), kinetically hindering the segregation and structural transformation[29].

To elucidate the origin of the pronounced difference in Fe segregation behavior between the two surfaces, ELF and COHP analyses were performed on the migrating Fe atom. On the ZCAFG-HEO surface, Fe migration is analyzed over an octahedral Ga_L site (with similar analysis over Al_L site provided in Figure S29), whereas over an octahedral Fe_L atom on the ZF-LEO surface. Bader charge analysis combined with ELF reveals that the Ga_L atom in ZCAFG-HEO surface donates 1.47 |e| to neighboring O atoms, exhibiting stronger electron-donating ability than the Fe_L atom in ZF-LEO surface (Fig. 5b). It results in more localized charge and stronger electronic interaction around Ga_L and O. Consequently, charge depletion of the migrating Fe decreases from 0.96 |e| to 0.58 |e|, and the -ICOHP value for the Fe-O bond decreases from 1.85 eV to 1.35 eV (Fig. 5c). The significantly weakened stabilization of migrating Fe atom leads to a higher migration barrier on the ZCAFG-HEO surface, thereby effectively stabilizing the Fe sites within the spinel lattice and sustaining high methanol selectivity in CO_2 hydrogenation (Fig. 5d). These theoretical findings reveal that incorporating highly oxyphilic B-site cations (Al, Ga) into the bulk of high-entropy spinel plays a crucial role in stabilizing active Fe sites, thereby preserving the durable spinel structure and suppressing segregation and carburization. This

electronic and structural stabilization mechanism is essential for achieving durable and selective methanol synthesis from CO_2 hydrogenation.

Conclusions

In this work, a spinel high-entropy oxide catalyst (ZCAFG-HEO) is rationally synthesized and applied in CO_2 hydrogenation to methanol for the first time. Comprehensive structural characterizations reveal that ZCAFG-HEO exhibits pronounced lattice distortion and nanoscale grain refinement compared to LEO and MEO catalysts, endowing its surface with a large number of reactive sites. Moreover, the incorporation of oxyphilic metals within HEO induces substantial charge redistribution, which reinforces metal-oxygen bonding and enhancing lattice robustness. Benefiting from these structural and electronic attributes, ZCAFG-HEO achieves high methanol synthesis activity with STY of 381 $g_{MeOH}{\cdot}kg_{cat}^{-1}{\cdot}h^{-1}$, which is 6.5-fold that of ZF-LEO and 2.2-fold that of ZCFG-MEO at the same reaction conditions. More remarkably, ZCAFG-HEO maintains exceptional catalytic stability over 120 h of continuous operation, whereas LEO and MEO catalysts suffer from rapid deactivation within merely 5 h. After optimizing the reaction conditions, ZCAFG-HEO delivers an unprecedented methanol STY of 498 $g_{MeOH}{\cdot}kg_{cat}^{-1}{\cdot}h^{-1}$ at 73.3% selectivity, on par with state-of-art oxide-based catalysts. *In-situ* characterizations elucidate that ZF-LEO undergoes progressive pathway shift from methanol synthesis to RWGS and methanation due to irreversible structural transformation from $ZnFe_2O_4$ spinel into Fe_3O_4 and Fe_5C_2 under CO_2 hydrogenation conditions, which serve as active sites for RWGS and FTS, accounting for the inferior methanol selectivity and poor stability. In sharp contrast, the structurally stable ZCAFG-HEO preserves the selective methanol synthesis pathway throughout the reaction, enabling consistent high performance. Theoretical calculations further reveal that the substantial charge redistribution within HEO kinetically hinders the migration of Fe, thus inhibiting the formation of Fe_3O_4 and Fe_5C_2. This stabilization mechanism is essential for achieving durable and selective methanol synthesis from CO_2 hydrogenation. This work not only opens a reliable avenue toward high-performance and durable CO_2 hydrogenation catalytic systems, but also provides atomic-level insights into the origin of the high-entropy effect in governing catalytic activity and stability, providing valuable theoretical guidance for the rational design of advanced high-entropy oxide catalysts.

Declarations

Data availability

The data that support the findings of this study are available in the paper and its Supplementary Information.

Acknowledgements

The authors thank the Coal-Major Project (2026ZD1703701), National Key Research and Development Program of China (2022YFA1504700), National Natural Science Foundation of China (U23A20112,

22308266), Foundation of Shanxi Key Laboratory of coal-based Synthetic Oil Product Testing (CbCZ202502), Natural Science Foundation of Wuhan (2026040301020033), Fundamental Research Funds for the Central Universities (2042026fg0047), Key Research and Development Program of Shandong Province (2025GNKJHZ0402). And we thank the Core Facility of Wuhan University for TEM and XPS tests. The numerical calculations were performed at the Supercomputing Center of Wuhan University.

Author contributions

M.D., X.G and D.X. conceived and supervised the project. S.H and T.Z. wrote the paper. G.H., Y.L., R.H., H.Z., J.P., H.Y., Y.W. and C.C. conducted the experimental work. All authors discussed the results and contributed to the final paper.

Competing interests

The authors declare no competing interests.

References

1. Zhong J et al (2020) State of the art and perspectives in heterogeneous catalysis of CO_2 hydrogenation to methanol. Chem Soc Rev 49:1385–1413
2. Jiang X, Nie X, Guo X, Song C, Chen J (2020) Recent advances in carbon dioxide hydrogenation to methanol via heterogeneous catalysis. Chem Sci 120:7984–8034
3. Olah G (2005) Beyond oil and gas: The methanol economy. Angew Chem Int Ed 44:2636–2639
4. Bai S et al (2021) Homogeneous and heterogeneous catalysts for hydrogenation of CO_2 to methanol under mild conditions. Chem Soc Rev 50:4259–4298
5. Harkou E, Wang H, Manos G, Constantinou A, Tang (2025) J. Advances in catalyst and reactor design for methanol steam reforming and PEMFC applications. Chem Sci 16:3810–3831
6. Sun X, Yan B (2025) Emerging strategies in engineering Cu-ZnO interfacial sites for CO_2 -to-methanol: Mechanistic advances, challenges, and opportunities. ACS Catal 15:18282–18304
7. Wang J et al (2017) A highly selective and stable ZnO-ZrO_2 solid solution catalyst for CO_2 hydrogenation to methanol. Sci Adv 3:e1701290
8. Wang J et al (2019) High-performance M_aZrO_x (M_a=Cd, Ga) solid-solution catalysts for CO_2 hydrogenation to methanol. ACS Catal 9:10253–10259
9. Zhang X et al (2021) Reaction-driven surface reconstruction of $ZnAl_2O_4$ boosts the methanol selectivity in CO_2 catalytic hydrogenation. Appl Catal B 284:119700
10. Zhang J et al (2025) Revealing the active phase of $ZnFe_2O_4$ catalyst for CO_2 hydrogenation to methanol. Appl Catal B 378:125532

11. Wang M et al (2024) Spinel nanostructures for the hydrogenation of CO_2 to methanol and hydrocarbon chemicals. J Am Chem Soc 146:14528–14538
12. Yang H et al (2024) Tuning the selectivity of CO_2 hydrogenation to alcohols by crystal structure engineering. Chem 10:2245–2265
13. Araújo TP, Mitchell S (2024) Pérez Ramírez, J. Design principles of catalytic materials for CO_2 hydrogenation to methanol. Adv Mater 36:2409322
14. Han X et al (2024) Rational design of catalysts with spinel nanostructures for thermal-driven C1 conversion. ACS Catal 14:9812–9828
15. Orege JI, Wei J, Ge Q, Sun J (2023) Spinel-structured nanocatalysts: New opportunities for CO_2 hydrogenation to value-added chemicals. Nano Today 51:101914
16. Feng W et al (2021) Insights into bimetallic oxide synergy during carbon dioxide hydrogenation to methanol and dimethyl ether over $GaZrO_x$ oxide catalysts. ACS Catal 11:4704–4711
17. Li K, Chen JG (2019) CO_2 hydrogenation to methanol over ZrO_2 -containing catalysts: Insights into ZrO_2 induced synergy. ACS Catal 9:7840–7861
18. Zhang P et al (2022) Boosting CO_2 hydrogenation performance for light olefin synthesis over $GaZrO_x$ combined with SAPO-34. Appl Catal B 305:121042
19. Tsoukalou A et al (2019) Structural evolution and dynamics of an In_2O_3 catalyst for CO_2 hydrogenation to methanol: An operando XAS-XRD and in situ TEM study. J Am Chem Soc 141:13497–13505
20. Wang J et al (2021) CO_2 hydrogenation to methanol over In_2O_3 -based catalysts: From mechanism to catalyst development. ACS Catal 11:1406–1423
21. Wang Y et al (2021) Visualizing element migration over bifunctional metal-zeolite catalysts and its impact on catalysis. Angew Chem Int Ed 60:17735–17743
22. Liu C et al (2025) Advances in high entropy oxides: synthesis, structure, properties and beyond. Prog Mater Sci 148:101385
23. Akrami S, Edalati P, Fuji M, Edalati K (2021) High-entropy ceramics: Review of principles, production and applications. Mater Sci Eng R Rep 146:100644
24. Albedwawi SH, AlJaberi A, Haidemenopoulos GN, Polychronopoulou K (2021) High entropy oxides-exploring a paradigm of promising catalysts: A review. Mater Des 202:109534
25. Tomboc GM et al (2022) Stabilization, characterization, and electrochemical applications of high-entropy oxides: Critical assessment of crystal phase–properties relationship. Adv Funct Mater 32:2205142
26. Ma Y et al (2021) High-entropy energy materials: Challenges and new opportunities. Energy Environ Sci 14:2295–2883
27. Zou J, Tang L, He W, Zhang X (2024) High-entropy oxides: Pioneering the future of multifunctional materials. ACS Nano 18:34492–34530

28. Pan Y, Liu J, Tu T, Wang W, Zhang G (2023) High-entropy oxides for catalysis: A diamond in the rough. Chem Eng J 451:138659
29. Li Y et al (2023) Cu-based high-entropy two-dimensional oxide as stable and active photothermal catalyst. Nat Commun 14:3171
30. Liu S et al (2025) Entropy-driven structural evolution in ceramic oxides. J Am Chem Soc 147:27685–27697
31. Strasser P et al (2010) Lattice-strain control of the activity in dealloyed core–shell fuel cell catalysts. Nat Chem 2:454–460
32. Hu J et al (2026) Rare-earth element-induced charge redistribution in high-entropy alloys toward highly stable oxygen evolution catalysis. ACS Nano 20:9147–9158
33. Zou X et al (2024) Interstitial oxygen acts as electronic buffer stabilizing high-entropy alloys for trifunctional electrocatalysis. Adv Mater 36:2412954
34. Zhang M et al (2025) High entropy spinel oxide $(Ni_{0.2}Co_{0.2}Zn_{0.2}Cu_{0.2}Mg_{0.2})Fe_2O_4$ nanofibers for efficient oxygen evolution reaction. J Mater Chem A 13:1287–1301
35. Zhang M et al (2024) Designing water resistant high entropy oxide materials. Nat Commun 15:8306
36. Lee JD et al (2022) Facilitating hydrogen dissociation over dilute nanoporous Ti-Cu catalysts. J Am Chem Soc 144:16778–16791
37. Kang H et al (2023) Generation of oxide surface patches promoting H-spillover in $Ru/(TiO_x)MnO$ catalysts enables CO_2 reduction to CO. Nat Catal 6:1062–1072
38. Bhan A, Gounder R, Macht J, Iglesia E (2008) Entropy considerations in monomolecular cracking of alkanes on acidic zeolites. J Catal 253:221–224
39. Xu D et al (2025) Tailored Fe catalyst microenvironment for highly efficient syngas conversion to olefins with low CO_2 emissions. Sci Bull 70:3803–3811
40. Chang Q et al (2018) Relationship between iron carbide phases (ε-Fe_2C, Fe_7C_3, and χ-Fe_5C_2) and catalytic performances of Fe/SiO_2 Fischer-Tropsch catalysts. ACS Catal 8:3304–3316
41. Ding X, Zhu M, Sun B, Yang Z, Han Y (2024) An overview on dynamic phase transformation and surface reconstruction of iron catalysts for catalytic hydrogenation of CO_x for hydrocarbons. ACS Catal 14:6137–6168
42. Wang X et al (2024) Breaking the activity-selectivity trade-off of CO_2 hydrogenation to light olefins. *Proc. Natl. Acad. Sci. U. S. A.* 121, e2408297121
43. Shi Y, Gao W, Liu G, Tsubaki N (2025) A review of CO_2 hydrogenation to liquid fuels. Chemsuschem 18:e202402756
44. Liu T, Xu D, Wu D, Liu G, Hong X (2021) Spinel $ZnFe_2O_4$ regulates copper sites for CO_2 hydrogenation to methanol. ACS Sustain Chem Eng 9:4033–4041
45. Feng Z et al (2023) Asymmetric sites on the $ZnZrO_x$ catalyst for promoting formate formation and transformation in CO_2 hydrogenation. J Am Chem Soc 145:12663–12672

46. Zhao H et al (2022) The role of Cu_1-O_3 species in single-atom Cu/ZrO_2 catalyst for CO_2 hydrogenation. Nat Catal 5:818–831
47. Xu D et al (2021) Advances in higher alcohol synthesis from CO_2 hydrogenation. Chem 7:849–881

Figures

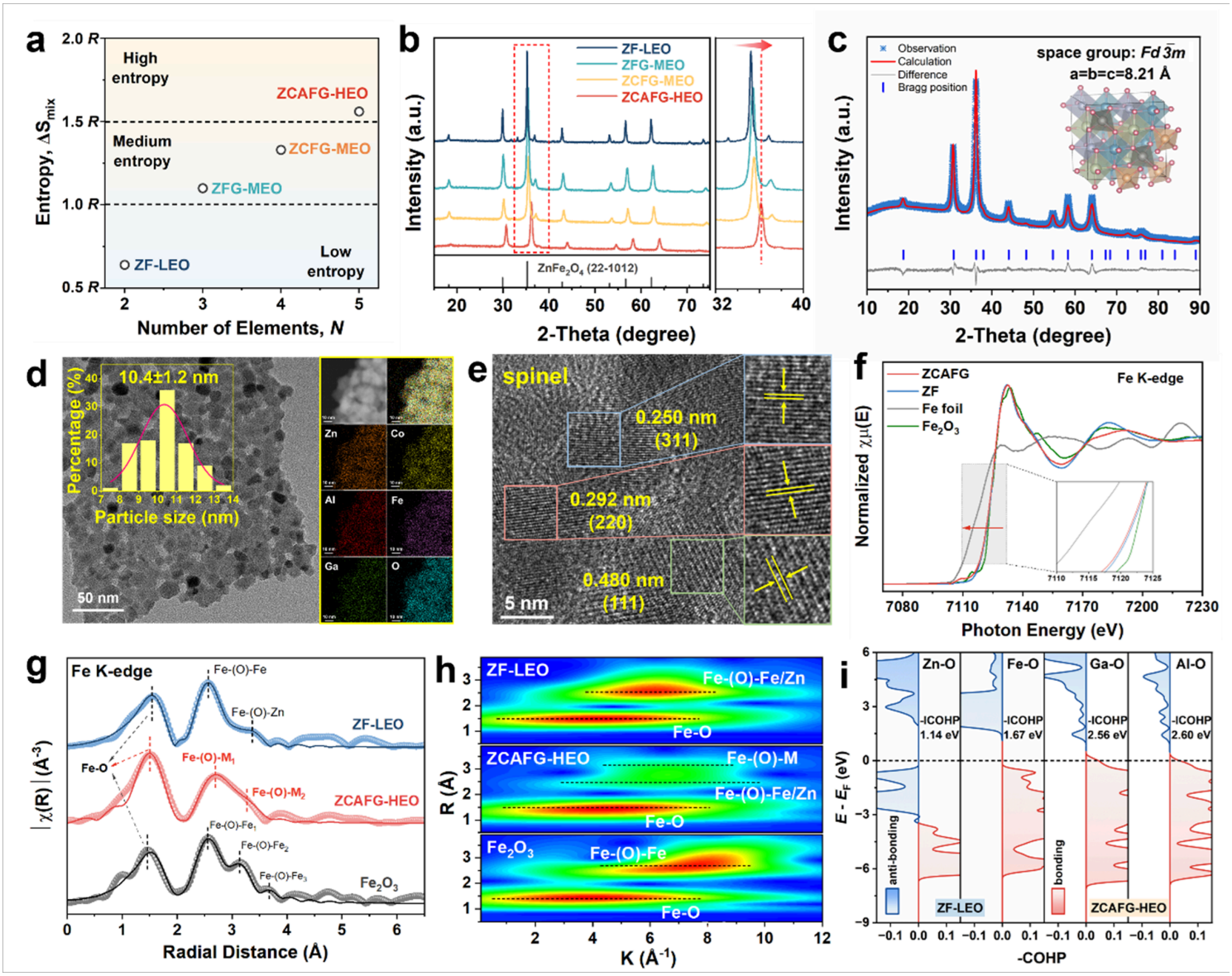


Figure 1

Structural characterizations of spinel catalysts. (a) Mixed configuration entropy. (b) XRD patterns and corresponding magnified views in the range of 32-40 degree (2-Theta). (c) Rietveld refinement XRD pattern of ZCAFG-HEO catalyst. (d) TEM image, corresponding particle size distribution and EDS mapping, and (e) HRTEM image of ZCAFG-HEO catalyst. (f) Fe K-edge XANES spectra, (g) fittings of the Fe K-edge Fourier-transformed intensities of EXAFS spectra and (h) Fe K-edge wavelet transform (WT)-EXAFS spectra of ZF-LEO and ZCAFG-HEO catalysts. (i) COHP analysis between O and surface metals.

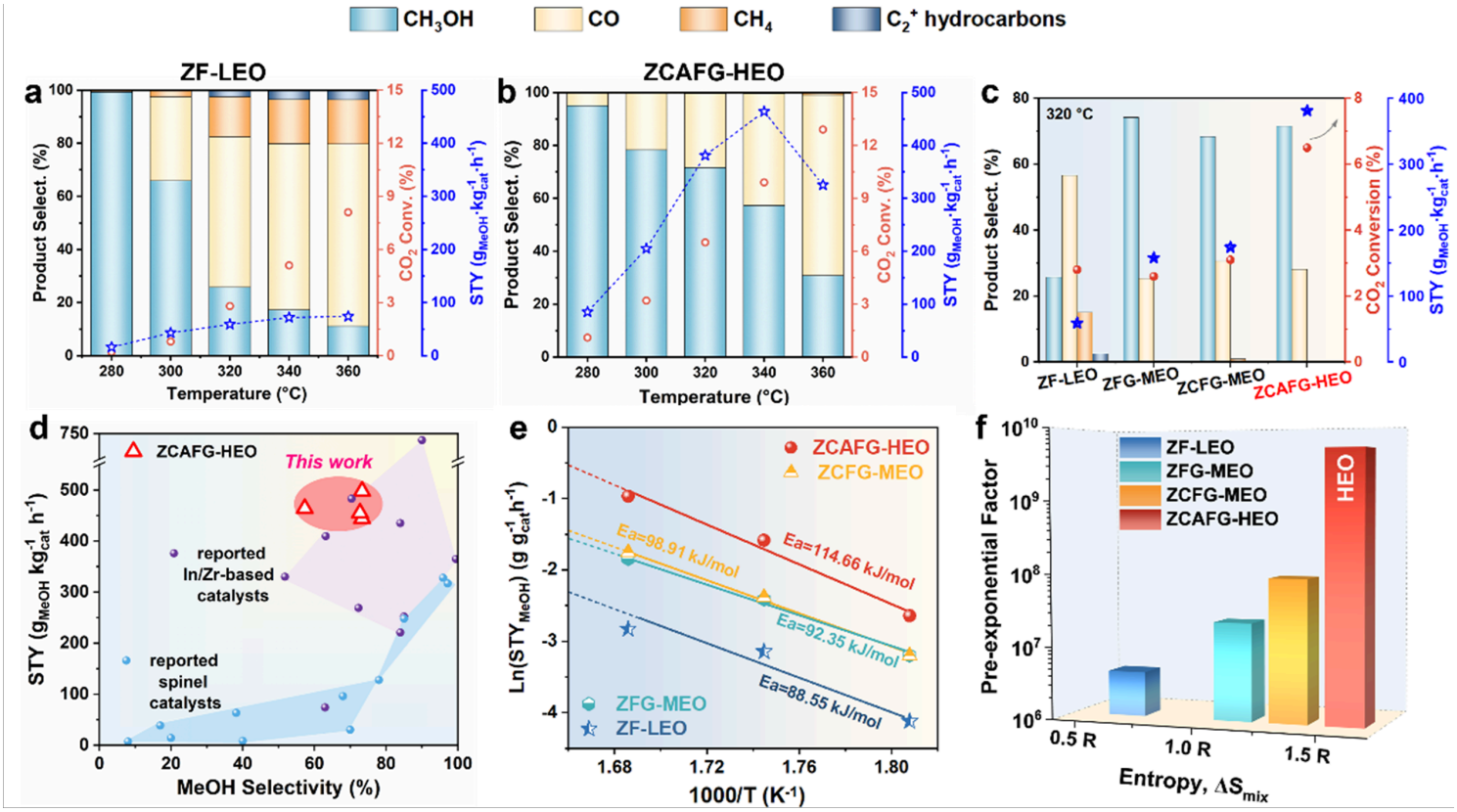


Figure 2

Catalytic performance of CO_2 hydrogenation to methanol. CO_2 conversion, product selectivity and methanol STY of (a) ZF-LEO and (b) ZCAFG-HEO. (c) Catalytic performance comparison of all spinel catalysts at 320 °C. (d) Catalytic performance comparison of ZCAFG-HEO catalyst with reported advanced oxide-based catalysts. (e) Determination of apparent activation energy of methanol synthesis. (f) Configuration entropy and pre-exponential factor of catalysts. Reaction conditions: 5 MPa, 24,000 $mL \cdot g^{-1} \cdot h^{-1}$, $CO_2/H_2/N_2$=24/72/4.

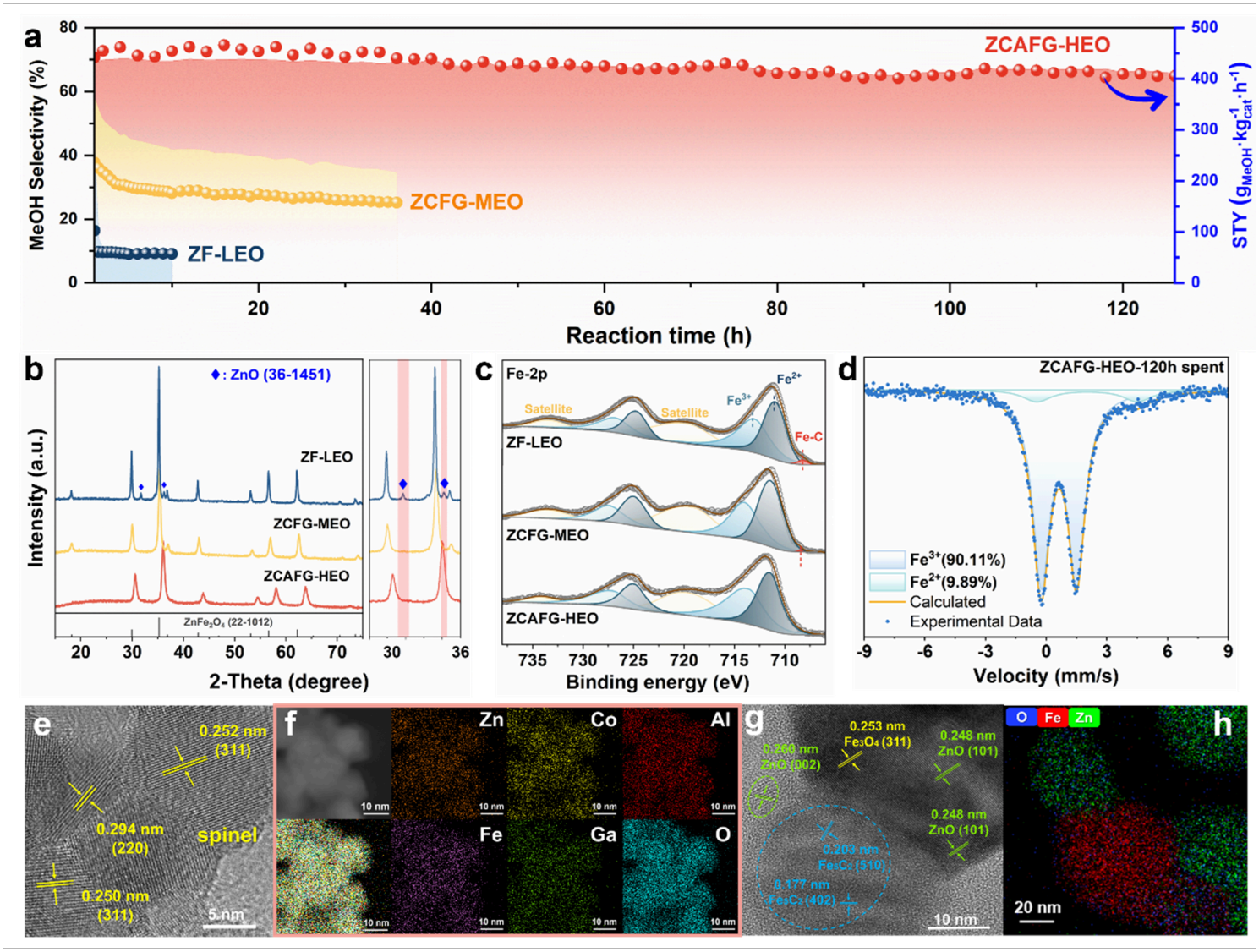


Figure 3

Investigation into catalyst stability. (a) CO_2 hydrogenation stability test of ZF-LEO, ZCFG-MEO and ZCAFG-HEO catalysts. Reaction conditions: 5 MPa, 36,000 $mL·g^{-1}·h^{-1}$, 320 °C, $CO_2/H_2/N_2$=24/72/4. (b) XRD patterns and (c) Fe 2p XPS spectra of ZF-LEO, ZCFG-MEO, and ZCAFG-HEO catalysts. (d) Mössbauer spectrum of ZCAFG-HEO. HRTEM and EDS mapping images of (e, g) ZCAFG-HEO and (f, h) ZF-LEO.

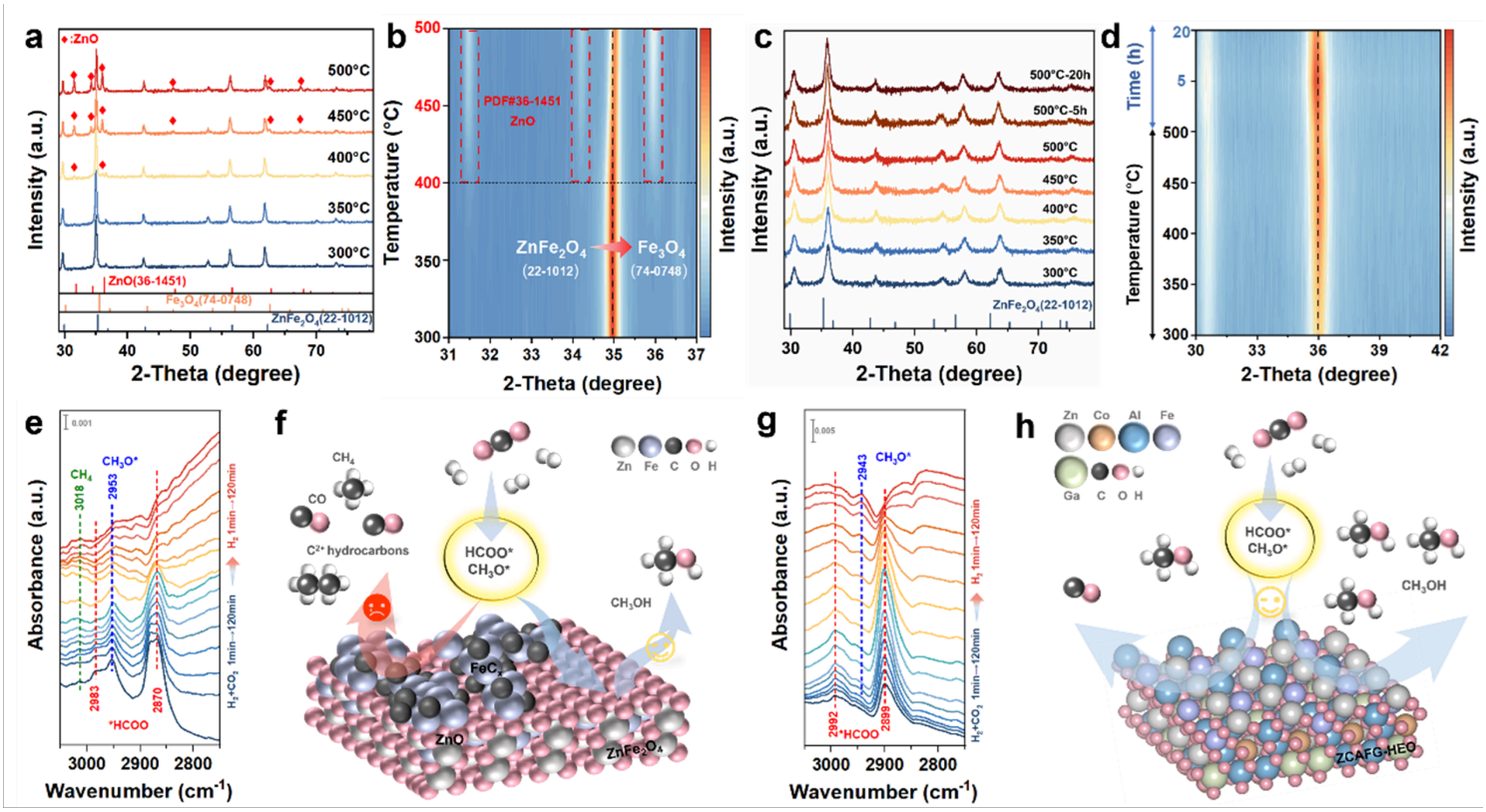


Figure 4

Evolution of Catalyst Structure and Reaction Pathway. *In-situ* CO_2 hydrogenation XRD patterns and corresponding magnified views in the range of 31-37 degree (2-Theta) of (a-b) ZF-LEO and (c-d) ZCAFG-HEO. *In-situ* CO_2 hydrogenation DRIFTS spectra and corresponding schematic diagram of reaction pathway of (e-f) ZF-LEO and (g-h) ZCAFG-HEO.

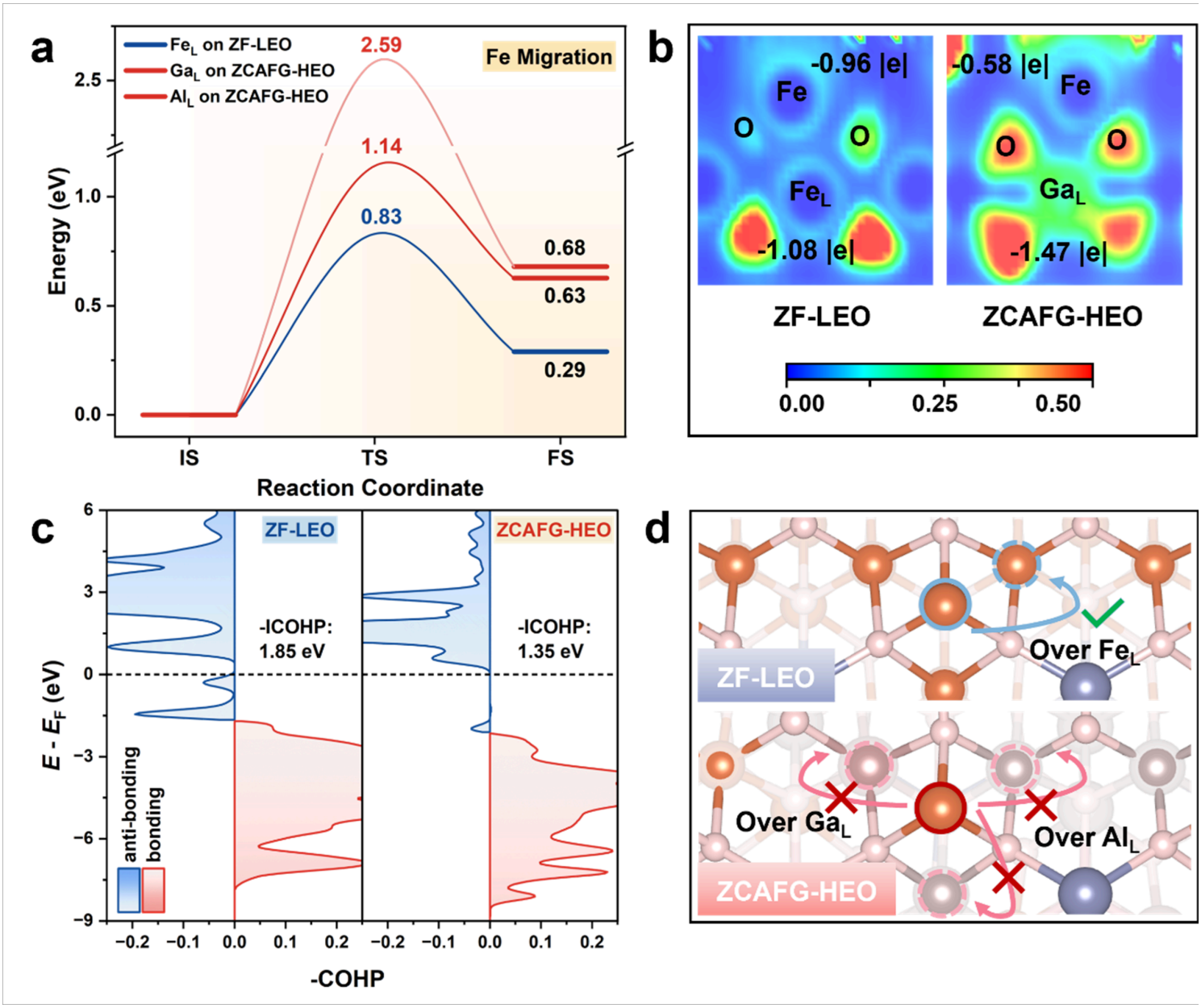


Figure 5

Stability Mechanism from theoretical perspective. (a) Potential energy surface for Fe segregation on ZF-LEO and ZCAFG-HEO surfaces. (b) Bader charge and the ELF slice for the side view of ZF-LEO and ZCAFG-HEO surfaces.(c) COHP analysis between the transition-state Fe atom and surface O atom. (d) Illustration of the Fe migration mechanism. Zinc (purple), Cobalt (pink), Aluminum (grey), Iron (yellow), Gallium (brown), and Oxygen (red).

Supplementary Files

This is a list of supplementary files associated with this preprint. Click to download.

- manuscriptSI.docx